

## **Tuning energetic properties through co-crystallisation: nitrotriazolone with 4,4'-bipyridine. A high pressure experimental and computational study.**

Imogen L. Christopher, Xiaojiao Liu, Hayleigh J. Lloyd, Craig L. Bull, Nicholas P. Funnel, Peter Portius, Adam A. L. Michalchuk, Stuart R. Kennedy, Colin R. Pulham,\* and Carole A. Morrison\*

### Supplementary Information

- S1. X-ray single crystal diffraction study
- S2. Computational modelling
- S3. Drop Weight Testing
- S4. Supplementary Characterisation Data for NTO·BIPY

## S1. X-ray single crystal diffraction study

Difference Fourier maps of NTO.BIPY, with the N1–H...N3 hydrogen atom removed (see main text for atom numbering), were calculated using WinGx to visualise the electron density hole it leaves behind. These images are shown in Figure S1 to confirm the formation of the co-crystal at ambient pressure conditions.

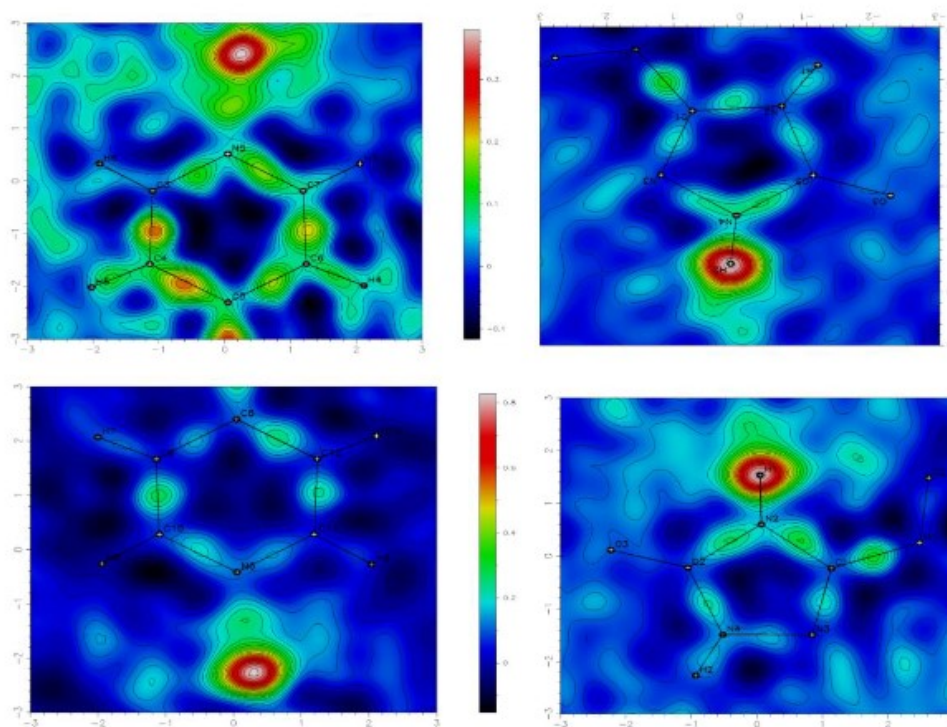


**Figure S1.** Difference Fourier maps of NTO.BIPY at ambient pressure, confirming the position of the hydrogen atom on N1.

**Table S1.** Crystallographic and structural refinement parameters of NTO.BIPY at 0 – 5.93 GPa.

Pressure	0 GPa
Temperature/K	293
Formula	C <sub>12</sub> H <sub>10</sub> N <sub>6</sub> O <sub>3</sub>
Formula Weight	286.25
Crystal System	<i>Monoclinic</i>
Space group	<i>P 2<sub>1</sub>/n</i>
<i>a</i> / Å	7.9440(7)
<i>b</i> /Å	5.7979(5)
<i>c</i> / Å	27.874(2)
$\alpha$ /°	90
$\beta$ /°	95.810(3)
$\gamma$ /°	90
<i>V</i> / Å <sup>3</sup>	1277.24
<i>Z</i>	4
<i>D<sub>c</sub></i> / g cm <sup>-3</sup>	1.489
$\mu$ /mm <sup>-1</sup>	0.113
<i>F</i> (000)	592
$\theta$ range/°	2.61- 26.34
Reflections collected	27388
Unique reflections	2576
Reflections <i>I</i> > 2 $\sigma$ ( <i>I</i> )	2576
<i>R</i> <sub>int</sub>	0.0207
goodness-of-fit ( <i>F</i> <sup>2</sup> )	1.137
<i>R</i> 1 ( <i>I</i> > 2 $\sigma$ ( <i>I</i> ))	0.0418
<i>wR</i> 2( <i>I</i> > 2 $\sigma$ ( <i>I</i> ))	0.1217
CCDC No.	2256439

Pressure	0.32 GPa	0.88 GPa	1.08 GPa	1.38 GPa	1.81 GPa	2.21 GPa
Temperature/K	289.5	296.1	296.1	275.6	296.1	296.0
Formula	C <sub>12</sub> H <sub>10</sub> N <sub>6</sub> O <sub>3</sub>	C <sub>12</sub> H <sub>10</sub> N <sub>6</sub> O <sub>3</sub>	C <sub>12</sub> H <sub>10</sub> N <sub>6</sub> O <sub>3</sub>	C <sub>12</sub> H <sub>10</sub> N <sub>6</sub> O <sub>3</sub>	C <sub>12</sub> H <sub>10</sub> N <sub>6</sub> O <sub>3</sub>	C <sub>12</sub> H <sub>10</sub> N <sub>6</sub> O <sub>3</sub>
Formula Weight	286.25	286.25	286.25	286.25	286.25	286.25
Crystal System	<i>Monoclinic</i>	<i>Monoclinic</i>	<i>Monoclinic</i>	<i>Monoclinic</i>	<i>Monoclinic</i>	<i>Monoclinic</i>
Space group	<i>P 2<sub>1</sub>/n</i>					
<i>a</i> / Å	7.9306(12)	7.6908(13)	7.6153(13)	7.6129(13)	7.4571(13)	7.3848(11)
<i>b</i> /Å	5.7908(7)	5.7271(4)	5.7099(4)	5.7121(10)	5.6784(4)	5.6634(4)
<i>c</i> / Å	27.809(4)	27.006(2)	26.8265(19)	26.809(10)	26.508(2)	26.3751(19)
$\alpha$ /°	90	90	90	90	90	90
$\beta$ /°	95.349(10)	90.719(9)	90.275(7)	90.448(18)	91.931(9)	92.598(7)
$\gamma$ /°	90	90	90	90	90	90
<i>V</i> / Å <sup>3</sup>	1271.5(3)	1189.4(2)	1166.5(2)	1165.8(5)	1121.8(2)	1102.0(2)
<i>Z</i>	4	4	4	4	4	4
<i>D<sub>c</sub></i> / g cm <sup>-3</sup>	1.495	1.599	1.630	1.631	1.695	1.725
$\mu$ /mm <sup>-1</sup>	0.113	0.121	0.123	0.123	0.128	0.130
<i>F</i> (000)	592	592	592	592.284	592	592
$\theta$ range/°	2.62-24.98	3.86-25.63	3.65-25.08	2.78-2.78	3.67-26.17	3.68-25.00

Reflections collected	7300	6652	6348	6538	6195	6162
Unique reflections	1996	2691	2997	2537	2934	3002
Reflections $I > 2\sigma(I)$	832	667	662	590	605	607
$R_{int}$	0.0472	0.0412	0.0527	0.0341	0.0385	0.053
goodness-of-fit ( $F^2$ )	1.090	1.122	1.090	1.1857	1.06	1.06
$R1 (I > 2\sigma(I))$	0.0411	0.0470	0.0472	0.0258	0.0404	0.0417
$wR2(I > 2\sigma(I))$	0.1229	0.1123	0.1028	0.0603	0.1019	0.1029
CCDC No.	2170541	2170530	2170537	2170536	2170539	2170540

Pressure	2.85 GPa	3.48 GPa	3.51 GPa	3.81 GPa	4.56 GPa	5.93 GPa
Temperature	298.0	298.0	292.9	300.8	298.4	298.4
Formula	C <sub>12</sub> H <sub>10</sub> N <sub>6</sub> O <sub>3</sub>	C <sub>12</sub> H <sub>10</sub> N <sub>6</sub> O <sub>3</sub>	C <sub>12</sub> H <sub>10</sub> N <sub>6</sub> O <sub>3</sub>	C <sub>12</sub> H <sub>10</sub> N <sub>6</sub> O <sub>3</sub>	C <sub>12</sub> H <sub>10</sub> N <sub>6</sub> O <sub>3</sub>	C <sub>12</sub> H <sub>10</sub> N <sub>6</sub> O <sub>3</sub>
Formula Weight	286.25	286.25	286.25	286.25	286.25	286.25
Crystal System	<i>Monoclinic</i>	<i>Monoclinic</i>	<i>Monoclinic</i>	<i>Monoclinic</i>	<i>Monoclinic</i>	<i>Monoclinic</i>
Space group	<i>P 2<sub>1</sub>/n</i>					
<i>a</i> /Å	7.2747(16)	7.2334(6)	7.2224(11)	7.1952(4)	7.1472(12)	7.0225(10)
<i>b</i> /Å	5.6382(6)	5.6302(4)	5.6283(4)	5.6211(3)	5.6110(4)	5.5811(4)
<i>c</i> /Å	26.176(3)	26.082(5)	26.087(2)	26.010(3)	25.939(2)	25.7121(18)
$\alpha^\circ$	90	90	90	90	90	90
$\beta^\circ$	93.556(12)	94.001(8)	94.048(7)	94.452(6)	94.766(8)	95.797(7)
$\gamma^\circ$	90	90	90	90	90	90
<i>V</i> /Å <sup>3</sup>	1071.6(3)	1059.6(2)	1057.8(2)	1048.79(16)	1036.6(2)	1002.59(18)
<i>Z</i>	4	4	4	4	4	4
<i>D<sub>c</sub></i> /g cm <sup>-3</sup>	1.774	1.794	1.797	1.813	1.834	1.896
$\mu$ /mm <sup>-1</sup>	0.134	0.136	0.136	0.137	0.139	0.143
<i>F</i> (000)	592	592	592	592	592	592
$\theta$ range/ $^\circ$	3.70-23.82	2.88-26.16	3.55-24.35	2.89-25.38	3.72-26.28	3.74-25.15
Reflections collected	5495	4897	5833	5605	5518	5470
Unique reflections	1871	1916	2240	2516	2739	2747
Reflections $I > 2\sigma(I)$	510	665	630	591	615	560
$R_{int}$	0.0655	0.036	0.0579	0.0286	0.0422	0.0524
goodness-of-fit ( $F^2$ )	1.086	1.085	1.10	1.097	1.133	1.06
$R1 (I > 2\sigma(I))$	0.0511	0.0428	0.0427	0.0250	0.0343	0.0317
$wR2(I > 2\sigma(I))$	0.1590	0.0704	0.1495	0.0620	0.1073	0.1281
CCDC No.	2170538	2170531	2170532	2170533	2170534	2170535

**Table S2.** Intermolecular hydrogen bond lengths (Å) of NTO.BIPY at selected pressure

$p/\text{GPa}$	$\text{N}_2\text{-H}\dots\text{N}'_4$	$\text{N}_1\text{-H}\dots\text{N}_3$
0	2.824(2)	2.741(2)
0.32	2.820(5)	2.730(5)
0.88	2.818(5)	2.707(4)
1.08	2.819(6)	2.697(5)
1.38	2.795(10)	2.680(9)
1.81	2.806(5)	2.665(4)
2.21	2.795(5)	2.644(4)
2.85	2.784(6)	2.613(5)
3.48	2.773(6)	2.599(6)
3.51	2.786(5)	2.622(4)
3.81	2.771(7)	2.590(7)
4.56	2.775(5)	2.605(4)
5.93	2.775(6)	2.579(5)

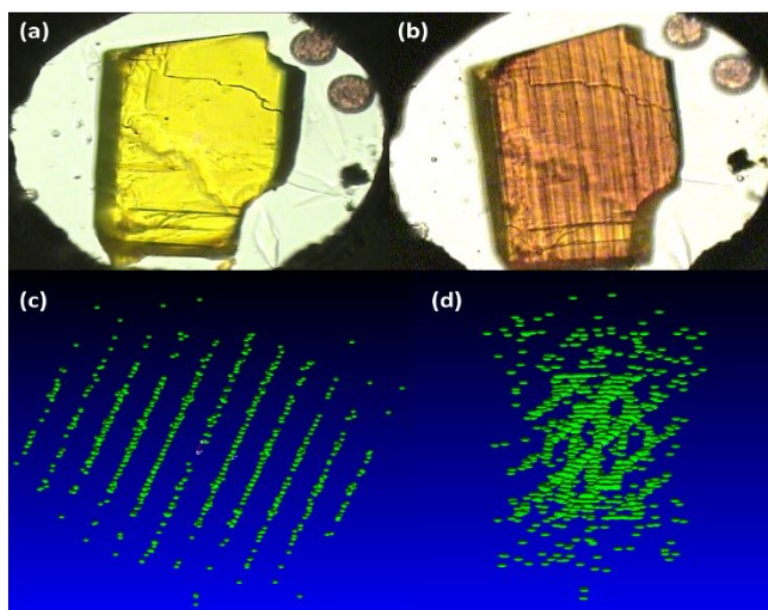


**Figure S3.** (a) Yellow crystal (*ca* 1.5 GPa) of NTO.BIPY converted to (b) orange (*ca* 6.0 GPa), with striations forming on the crystal surface potentially induced by multiple twinning. (c) Precession image of  $hk0$  zone of the orange crystal shows clear diffraction, while (d) diffraction on the  $0kl$  zone shows severe twinning. DAC scattering has been removed from images (c) and (d).

## S2. Computational Modelling

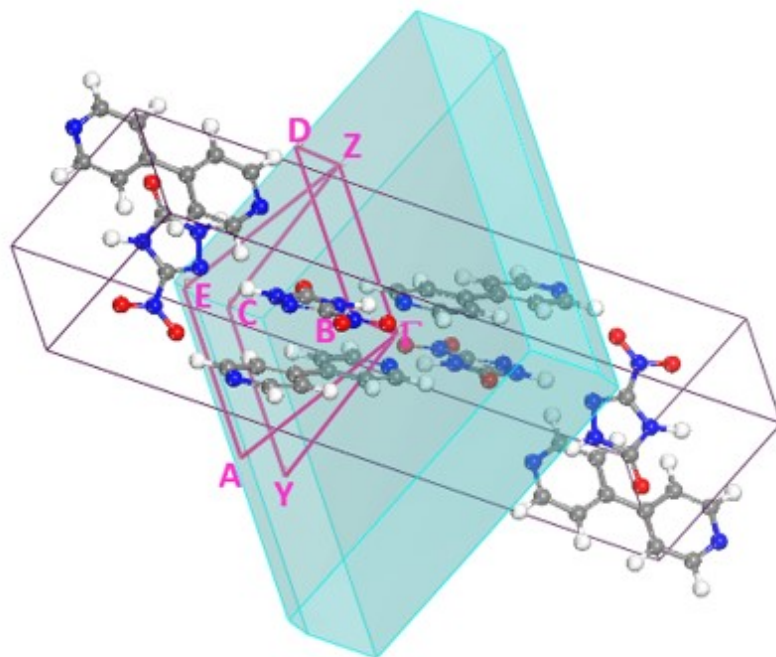
**Table S3** Percentage change of unit cell parameters for NTO.BIPY with increasing pressure, compared with experimentally-determined unit cells.

Pressure/GPa	a (Å)	b (Å)	c (Å)	$\beta$ (°)	V (Å <sup>3</sup> )
0	-1.45	+0.21	-1.53	-1.87	-2.52
1.81	+0.60	-0.51	-0.01	-1.12	+0.12
3.48	+1.36	-0.60	+0.07	-1.66	+0.98
5.93	+0.77	-0.51	-0.11	-1.22	+0.34

**Table S4** N1–D bond lengths ( $X_{\min}$ ) corresponding to lowest energy points on calculated PES (Fig. 4(a) in main text) with increasing pressure, along with N1–D expectation values  $\langle x \rangle$  from 1D Schrodinger equation solutions, and N1...N3 optimised bond lengths.

Pressure (GPa)	$X_{\min}$ (Å)	$\langle x \rangle$ (Å)	N1...N3 (Å)
0.00	1.078	1.094	2.751
1.77	1.086	1.103	2.664
3.48	1.108	1.130	2.590
5.93	1.156	1.160	2.548

(a)



(b)

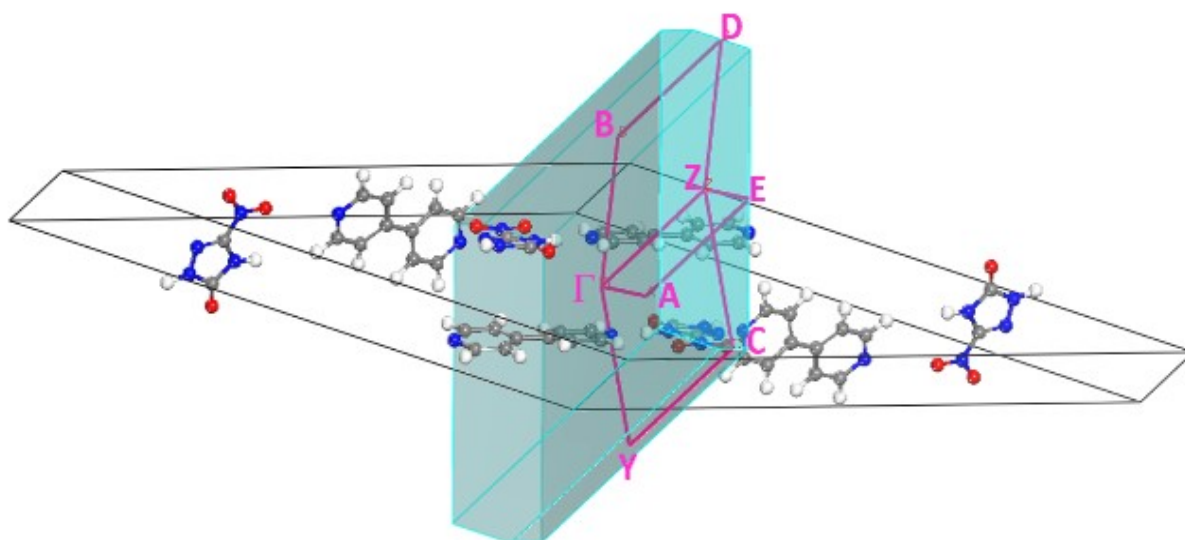


**Figure S4.** Visualisation of the Brillouin zone paths onto the real space (conventional and primitive) unit cells at (a) 0 GPa and (b) 5.93 GPa, plotted using Materials Studio.

To allow comparison of the vibrational up-pumping results for NTO.BIPY alongside other energetic materials, most notably  $\alpha$ -NTO,  $g(\omega)$  was first normalised according to the number of modes in the phonon bath (for NTO.BIPY, 68 modes were located below  $\Omega_{\max} = 210 \text{ cm}^{-1}$ ). The top of the phonon bath ( $\Omega_{\max}$ ) was identified based on the  $g(\omega)$  plot shown in Figure 9 of the main text, and the drop-off in centre of mass of displacement displayed by the eigenvectors, as shown in Figure S5. The resulting density of states was then up-pumped via a number of scattering routes which combine two lower frequencies ( $\omega_1, \omega_2$ ) to create a higher frequency mode ( $\omega_3$ ). Permitted phonon scattering pathways include:

1. External lattice phonon self-scattering (i.e.  $\omega_1 + \omega_1 \rightarrow \omega_3$ ), where  $\omega_3 = \frac{\omega_1}{2}$ . This is akin to overtone mode generation and creates new vibrational bands in the region  $0 - 2\Omega_{\max}$ .
2. External lattice phonon ( $\omega_1$ ) scattering with a so-called doorway mode ( $\omega_2$ , which resides between  $1 - 2\Omega_{\max}$ ) to create bands that fall between  $1 - 3\Omega_{\max}$ .
3. External lattice phonon ( $\omega_1$ ) scattering with an excited doorway mode ( $\omega_2$ , generated in step 2) to excite new bands that lie between  $1 - 3\Omega_{\max}$ .

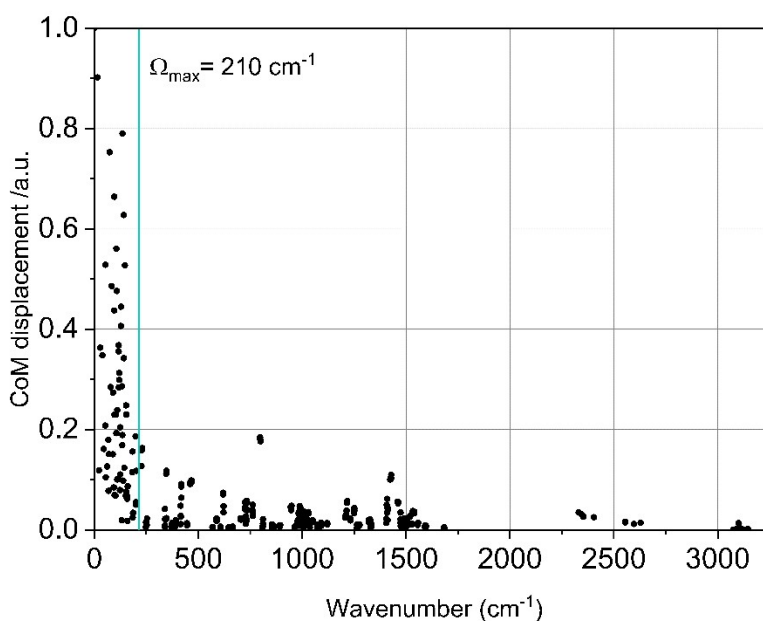


**Figure S5.** Average centre of mass displacements for the NTO and BIPY molecules in the ambient pressure unit cell of NTO·BIPY, as displayed by the eigenvectors of the vibrational modes.

The population density for the phonon bath modes is scaled according to  $T_{\text{shock}}$ , i.e. the super-heated phonon quasi-temperatures adopted to simulate the mechanical impact event, and obtained from the ratio of the bulk heat capacity ( $C_{\text{tot}}$ ) to the phonon heat capacity ( $C_{\text{ph}}$ ), as shown in Figure S6. This yields a value of 5.19; based on previous work a  $C_{\text{tot}}/C_{\text{ph}}$  ratio of 5.00 was set to 3278K (calculated from the adiabatic compression of a model organic crystal, see ref25 in main text). Thus  $T_{\text{shock}} = 3402 \text{ K}$  for NTO.BIPY. All non-lattice modes were populated to  $T=300 \text{ K}$ .

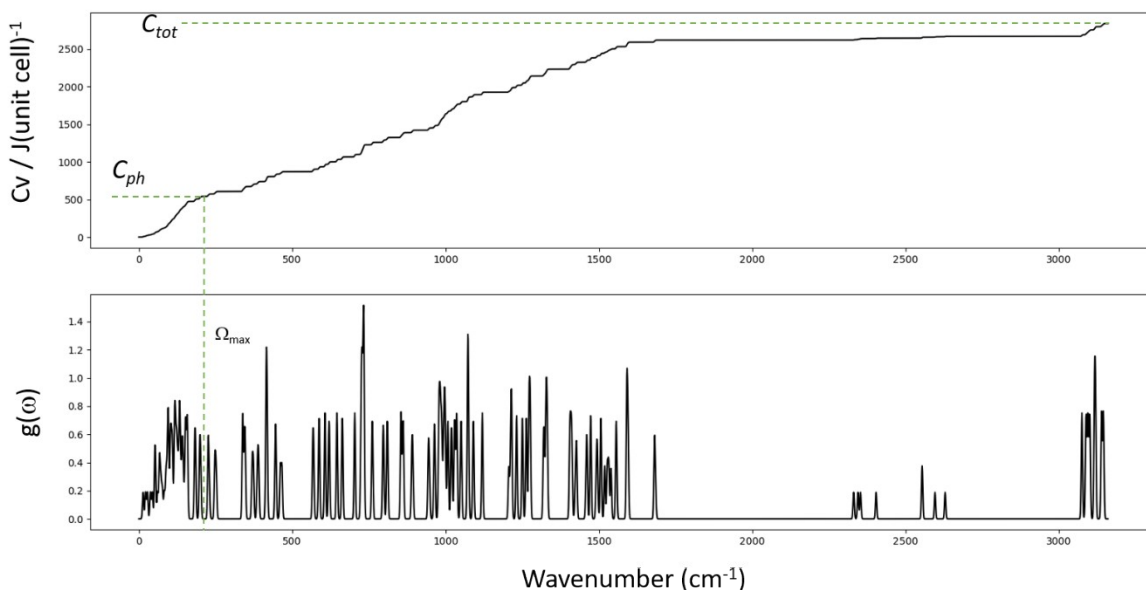


**Figure S6.** Cumulative heat capacities for ambient pressure NTO.BIPY. The position for the total ( $C_{tot}$ ) and phonon ( $C_{ph}$ ) heat capacities are shown.

The up-pumped multi-phonon density of states  $\Omega^{(2)}$  are subsequently projected onto the fundamental vibrational bands to identify how much of the up-pumped energy is ‘captured’ by the molecular vibrations. Finally, the resulting projected multi-phonon density of states is normalized with respect to the number of molecules ( $Z = 8$ ) contained in the unit cell, accounting for the localization of energy into individual molecules at this stage. For NTO.BIPY, four vibrational modes (marked with \* in Figure 9 of the main text) were excluded from the integration, as these vibrations were almost exclusively based on the non-energetic BIPY molecules.

**Table S7.** Parameters used to calculate the impact sensitivities of NTO and NTO.BIPY which are presented in Table 2.

Structure	$\Omega_{max} / \text{cm}^{-1}$	$Z(6+Y)$	Shock T / K	Up-pumped density/ $Z \times 10^3$ a.u.
$\alpha$ -NTO	204	64	2643	12.4
NTO.BIPY	210	68	3402	20.8

### S3. Impact Response Measurements

Data on the impact sensitivity for the NTO·BIPY adduct were obtained using the drop-weight tester at Sheffield. Briefly, the instrument uses a 0.936 kg weight that can be dropped from various heights ( $h$ ) onto the sample. The sample is supported by an anvil (4.12 kg). Both anvil and weight are composed of steel. The mass of typical samples ( $m_s$ ) ranges from 6 mg to 18 mg. The material is wrapped into stainless steel foil cut from 0.01 mm thin stock to the dimension of *ca.* 14 mm x 14 mm,  $m_c = 13$  mg to 16 mg, and then placed in the sample pit. The drop weight impacts the sample by a conically shaped face (surface area of *ca.* 70 mm<sup>2</sup>) that hits the centre of the tapered, circular, 12 mm wide and 3.2 mm deep sample pit. The rounded side walls of both impact cone and pit share a cone angle of 120°. The measurement was carried out without humidity control. Impact sensitivity data is usually given as the interpolated energy ( $E_{50}$ ) at which initiation occurs with a probability of 50%. The maximum drop

height for the tester, 90.5 cm, is equivalent to 8.3 J. An impact initiation energy of  $E_{50} = 5.5(\pm 0.2)$  J was measured for a large dataset (90 drops using, aluminium sample containers) of pure, untreated, synthesis-grade RDX obtained by the hexamine-nitric acid method, which compares well with data given elsewhere for this compound (J. Köhler *Explosives* 4<sup>th</sup> ed. 1993, p70; J. Akhavan *The Chemistry of Explosives* 3<sup>rd</sup> ed. 2011, p79; T. Klapötke *Chemistry of High Energy Materials* 2<sup>nd</sup> ed. 2012, p118, all quote 7.5 J). Sentencing of observations regarding the *go / no go* category is difficult if the visible and audible responses (flash, bang, smoke, smell, recoil, discolouration) are not clearly above the baseline defined by a non-reactive or non-energetic sample. For this reason, all impacts were audio-visually monitored by video recordings, and the results quantified based on a spectral analysis of the sound traces (see Figure S7) in combination with mass losses.

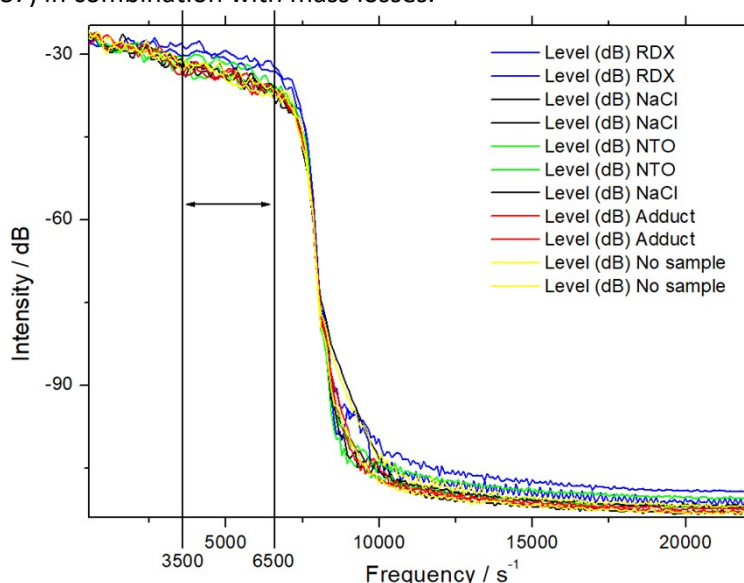


**Figure S7.** Sound spectra in the spectral range 80 Hz to 22 kHz. The spectra are derived from the sound traces covering the period 0.000 s to 0.700 s after drop weight impact. The limits of the region of sound intensity analysis are indicated by the double-headed arrow.

A base line sound intensity level was established by averaging over responses from the empty steel sample containers and sodium chloride samples, which gave  $I_{\text{ref}}^{\text{dB}} = -33.77$  dB, standard error  $\pm 0.16$  dB. A "go" impact was distinguished from a "no go" one if the sound level was above the upper  $2\sigma$  limit of the base line. According to this analysis, all RDX samples, and two NTO samples, were initiated with at least 95% certainty. The baseline sound intensity  $I_{\text{ref}}^{\text{dB}}$  can be used as a reference to compare the intensity ratios of absolute sound intensities (eqn. 1)

$$I_a / I_{\text{ref}} = 10^{(I^{\text{dB}} - I_{\text{ref}}^{\text{dB}})/10} \quad (\text{eqn. 1})$$

from which the energetic response is worked out by removing the baseline sound level  $I_{\text{ref}}$

$$I_{\text{EN}} = 10^{(I^{\text{dB}} - I_{\text{ref}}^{\text{dB}})/10} - 1 \quad (\text{eqn. 2})$$

The relative intensity arising from an energetic response can then be normalised to the average sample mass  $m_s^{\text{av}}$

$$I_{\text{EN}}^{\text{norm}} = m_s^{\text{av}} / m_s I_{\text{EN}} \quad (\text{eqn. 3})$$

to account for varying sample masses.

In order to add certainty to the sentence, a visual inspection of samples post impact as well as the video evidence was performed. Processes of material ejection upon impact can be clearly seen (Figure S9).

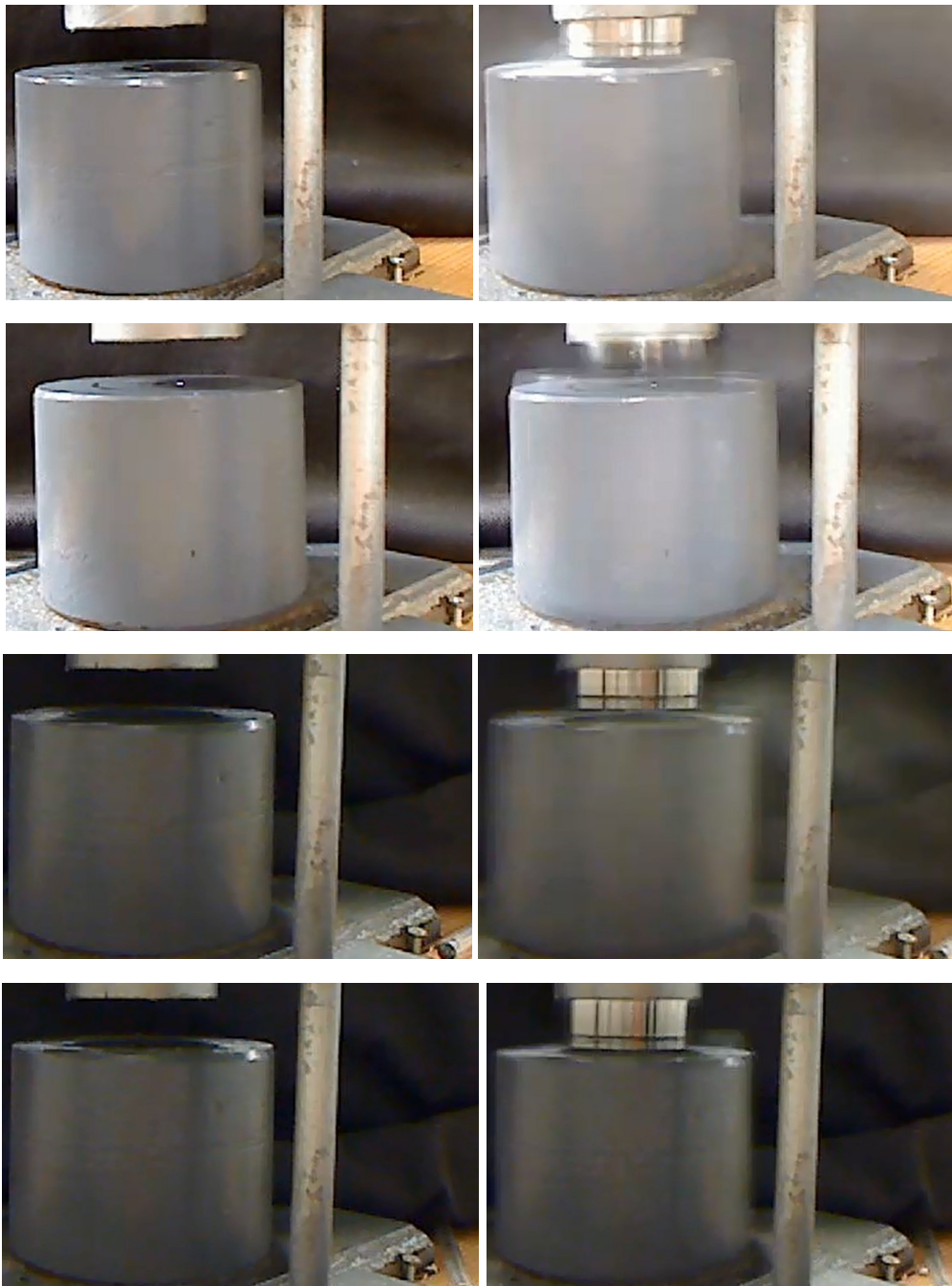


**Figure S9.** Video frames *before* (left), and *after impact* (right,), showing dust clouds arising from samples of RDX (1<sup>st</sup> row), NTO (2<sup>nd</sup> row) and NTO-BIPY (third row), but not from NaCl (4<sup>th</sup> row) .

The ejected material consists of sample container shreds as well as finely divided dust particles. In order to obtain an indication of the extent of a possible energetic response, masses before and after impact were determined. The recoverable mass after impact ( $m_r$ ) includes all particles left on the anvil and under the impact cone. The level of mass loss by ejection is treated in a fashion similar to that of the sound intensities. The level of mass loss of empty sample containers  $r_{ref} = \Delta m / m_c$  was found to be at 0.036 and this is removed from any mass losses due to energetic responses in the following way:

$$r^{\text{norm}} = (m_c + m_s - m_r + m_c r_{\text{ref}}) / m_s \quad (\text{eqn 4})$$

in which  $m_c$ ,  $m_s$  and  $m_r$  refer to the masses of the sample container, the sample, and the recovered mass, respectively. This treatment removes the effect of varying sample masses as well as changes to the sample container masses. The experimental data and derived quantities can be found in Table S5.

**Table S5.** Masses, sound intensities and normalised impact responses (uncertainty refers to the standard error (propagated) or estimates thereof).

Sample	$m_c$ / mg	$m_s$ / mg	$m_r$ / mg	$I^{\text{dB}}$ / dB	$I_{\text{EN}}$ / a.u.	$I_{\text{EN}}^{\text{norm}}$	uncert.	$r^{\text{norm}}$	uncert.
none	15	0	12	-34.3899	-	-	-	-	-
none	12	0	13.5	-33.3254	-	-	-	-	-
none	15	0	15	-33.1658	-	-	-	-	-
NaCl	15	28	42	-34.2292	-0.1013	-0.056	0.050	0.05	0.081
NaCl	16	18	30	-33.5155	0.0596	0.051	0.096	0.22	0.083
NaCl	14	18	31	-33.7330	0.0077	0.007	0.082	0.06	0.081
NaCl	21	29	48	-33.6217	0.0340	0.018	0.058	0.13	0.095
RDX1	16	17	8	-29.9041	1.4363	1.310	0.195	1.55	0.093
RDX2	14	18	5	-31.0586	0.8671	0.747	0.143	1.56	0.087
RDX3	16	17.5	6	-31.7724	0.5838	0.517	0.138	1.66	0.090
NTO1	15	12	12	-34.2236	-0.1001	-0.129	0.116	1.37	0.136
NTO2	15	8	5	-31.9178	0.5316	1.030	0.297	2.41	0.200
NTO3	13	6	11	-32.5551	0.3223	0.833	0.326	1.53	0.284
adduct1	15	12	12	-34.1772	-0.0904	-0.117	0.101	1.42	0.142
adduct2	15	10	18	-33.9862	-0.0495	-0.077	0.160	1.00	0.213
adduct3	13	8	8.5	-34.1919	-0.0935	-0.181	0.193	2.02	0.242

Plots of the normalised sound intensities and mass losses (Figure S8) clearly show that RDX initiates each time by giving rise to sound levels and extensive sample mass losses that are statistically above the background (>95% certainty). This is not the case for NTO, which did not produce sound in one instance, but did give rise to significant mass loss each time. The NTO·BIPY adduct, however, does not produce sound, but still undergoes extensive ejection of material after each impact. No discolouration or odour was noticeable.

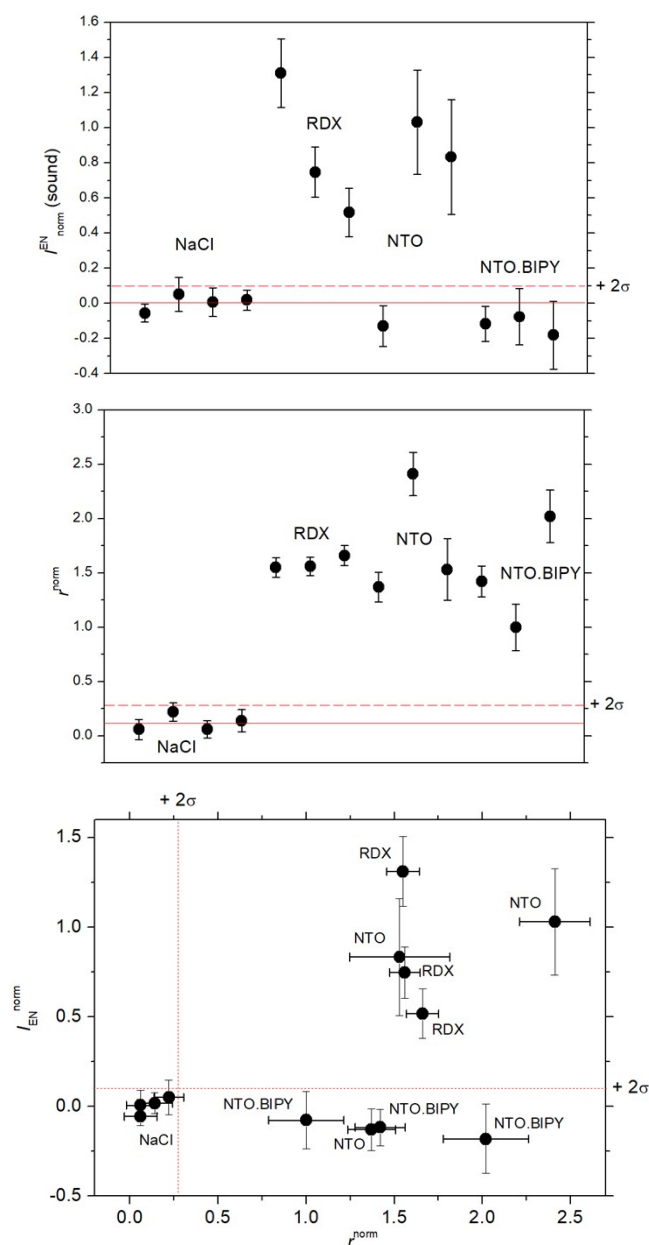


**Figure S8.** Comparative analysis of sound intensities (top), mass losses (middle), and a correlation involving both (bottom) for the substances NaCl, RDX, NTO and NTO·BIPY upon drop weight impact; the ‘go/no go’ boundary is denoted by the solid lines, the  $2\sigma$  margin above the average of the references by the dotted lines, while the error bars show the propagated estimated standard deviation.

The possibility of the NTO·BIPY material having undergone a reaction upon impact was investigated by infrared spectroscopy. Flaky material recovered after the drop weight impacted on one sample was mullied in paraffin and pasted onto NaCl windows. In comparison to the original material, the resultant spectra clearly show, apart from a change in the extent of the Christiansen effect (smaller band distortion, narrower bands pointing to a reduction in size of crystals), that no chemical reaction had taken place. The intensity of a few small bands ( $3416\text{ cm}^{-1}$ ,  $1584\text{ cm}^{-1}$  and  $612\text{ cm}^{-1}$ ) *decreased* upon impact compared to all other absorption bands (see Figure S12). These small bands are assigned to traces of adsorbed water. Nothing can be deduced concerning the ejected material as we were unable to recover it. It is therefore possible that, even though local heating may lead to the onset of

decomposition and gas evolution, the induced effects are too weak to either increase the chemical reaction rate, or allow propagation initially, which produces the observed dust clouds. The same argument holds true for the "no go" NTO sample.

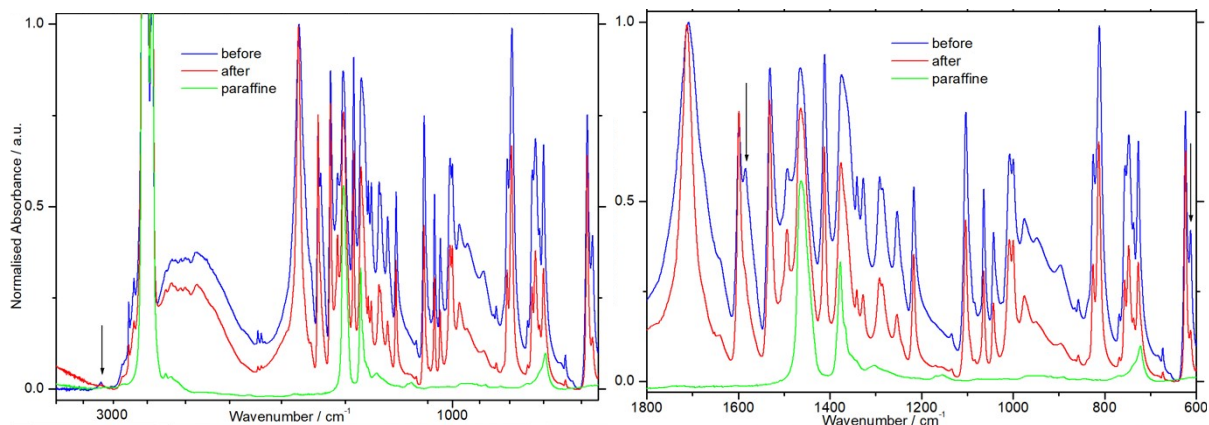


**Figure S12.** Impact reactivity analysis (IR spectra), 3400 to 600  $\text{cm}^{-1}$  (left), expanded range (1800 to 600  $\text{cm}^{-1}$ , right). Adsorbed water traces are indicated by black arrows. Spectra are normalised to the peak absorbance at 1709  $\text{cm}^{-1}$  for clarity (resolution 2  $\text{cm}^{-1}$ ).

### S4. Supplementary Characterisation Data for NTO·BIPY

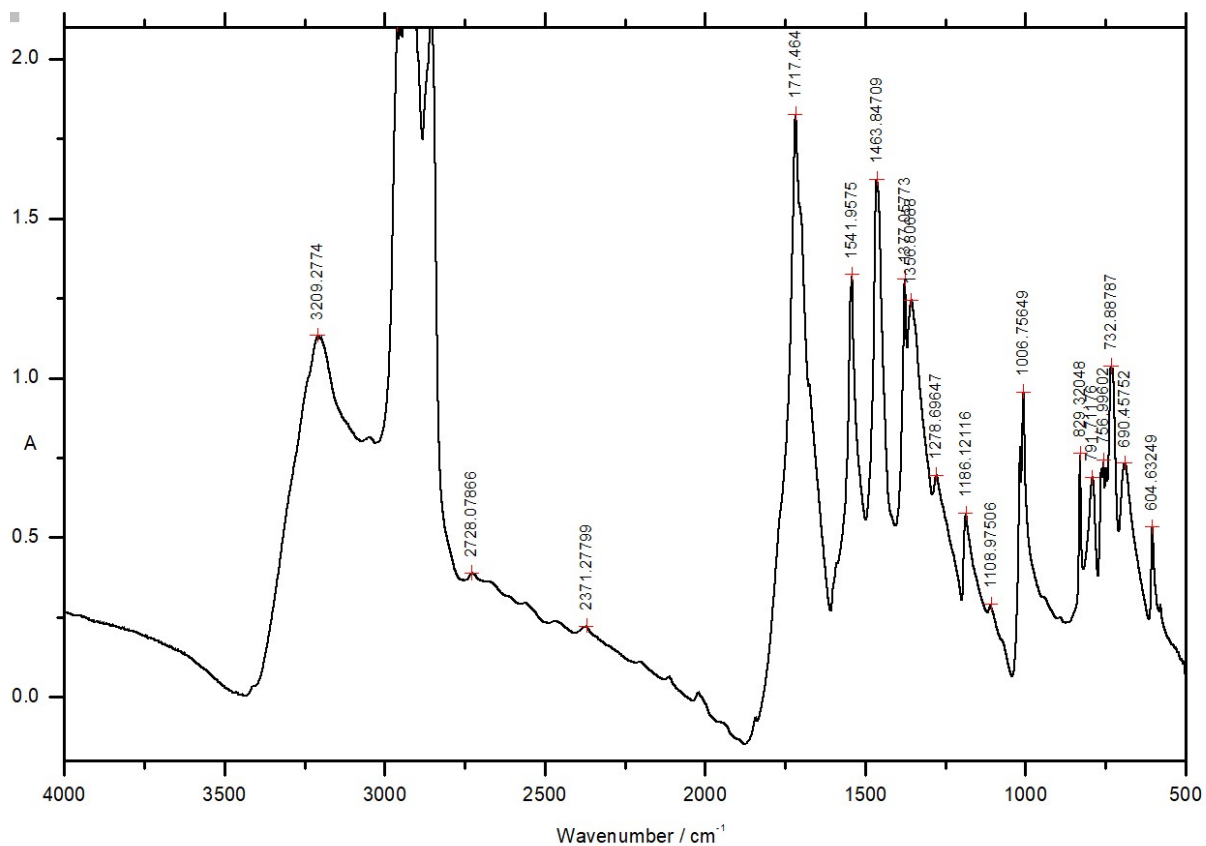
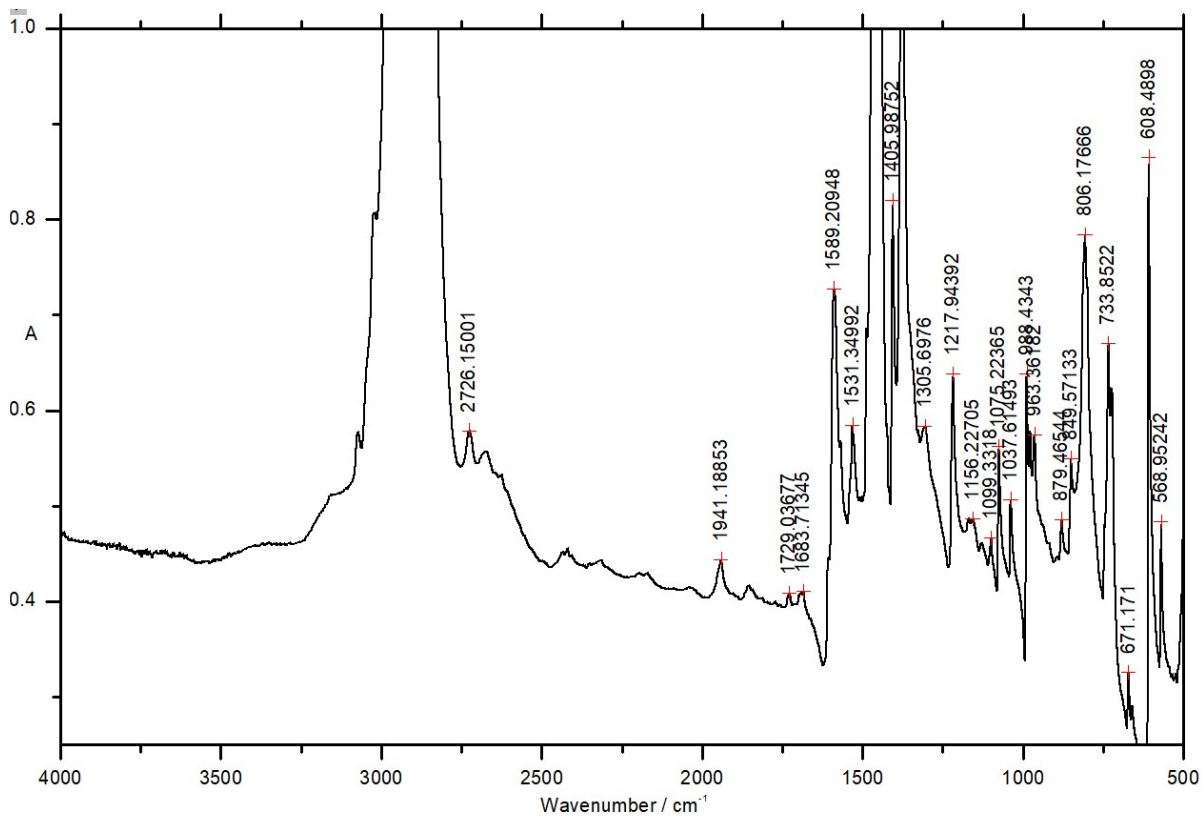
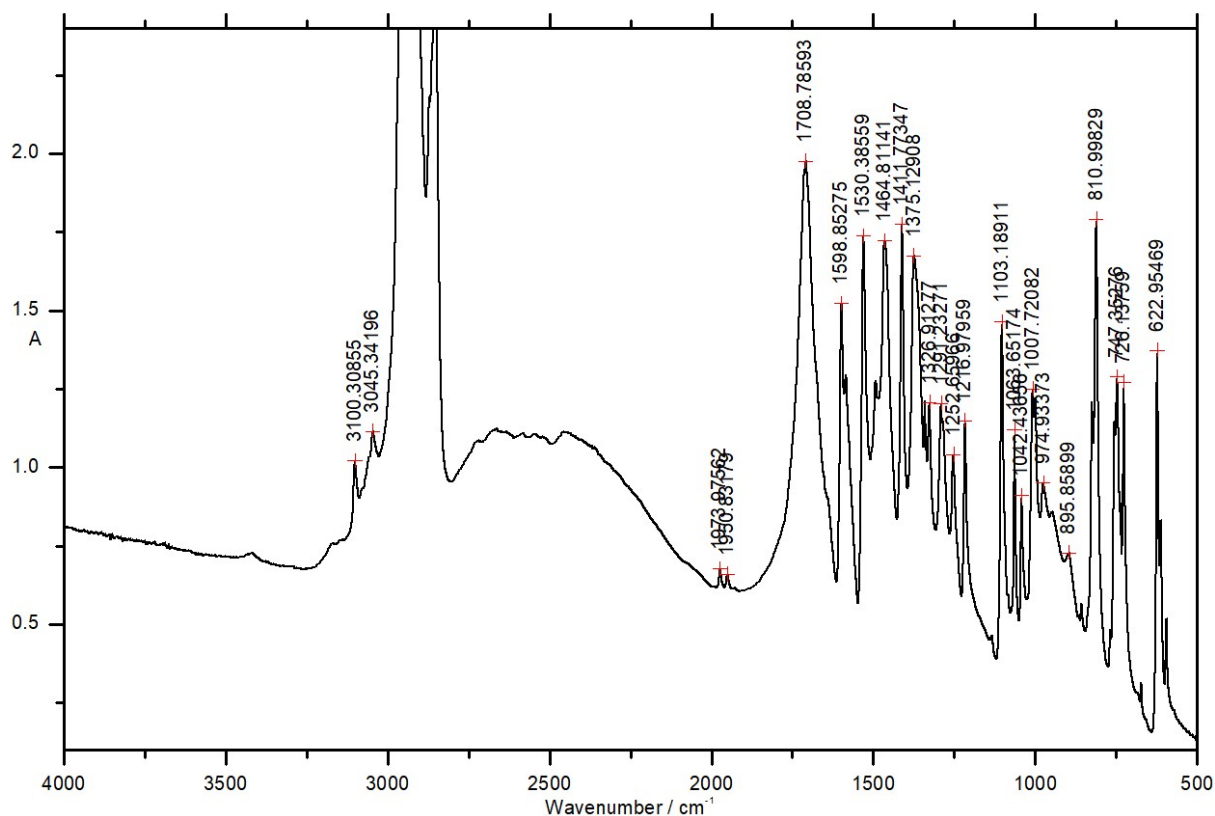


Figure S7. IR spectrum of a paraffin mull of NTO (resolution 2 cm<sup>-1</sup>).



**Figure S8.** IR spectrum of a paraffin mull of **4,4'-BIPY** (resolution 2 cm<sup>-1</sup>).



**Figure S9.** IR spectrum of a paraffin mull of **NTO·BIPY** (resolution 2 cm<sup>-1</sup>).

**Table S10.** Key infrared vibrational spectroscopy data

sample	$\nu(\text{C-H}) / \text{cm}^{-1}$	$\nu(\text{C=O}) / \text{cm}^{-1}$	$\nu(\text{N-H}) / \text{cm}^{-1}$	FWHM (N-H) / cm <sup>-1</sup>
<b>NTO·BIPY</b>	3100, 3045	1709	<i>ca.</i> 2550	<i>ca.</i> 250
<b>NTO</b>	-	1717	3209	<i>ca.</i> 210
<b>4,4'-BIPY</b>	3072, 3021	-	-	-

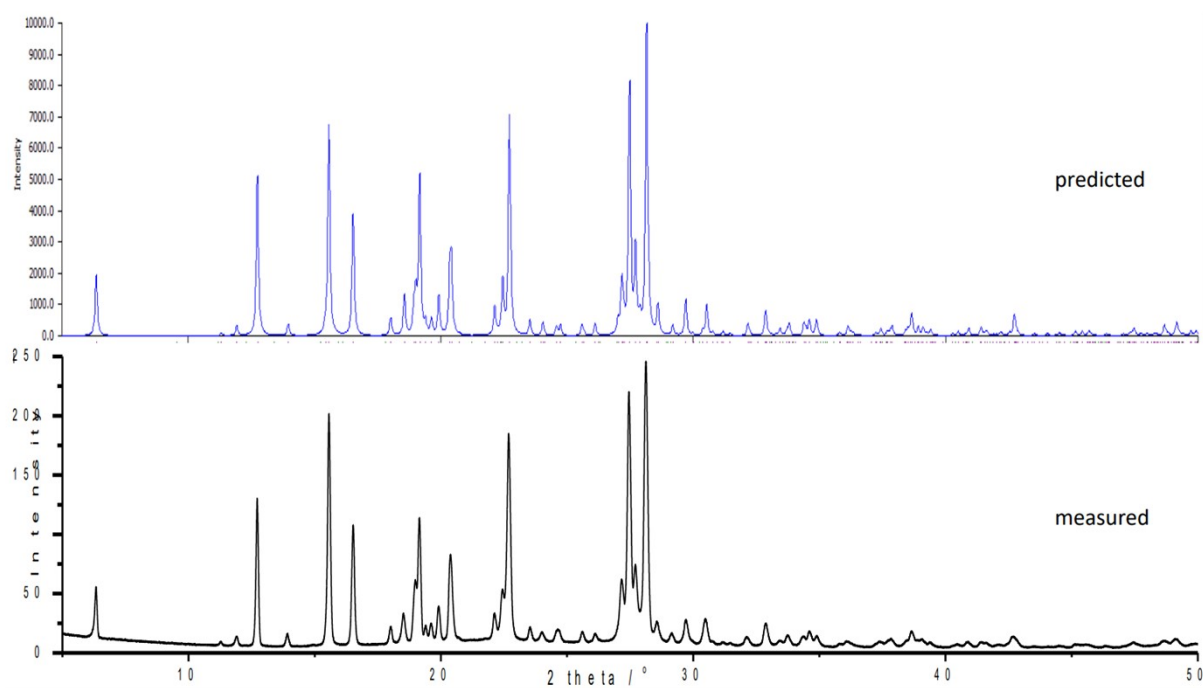


**Figure S10.** X-ray powder diffractogram (PXRD) of freshly synthesised **NTO-BIPY** (black), and the predicted PXRD based on the crystal structure at r.t.p. (blue).